



## Cascading reaction of arginase and urease on a graphene-based FET for ultrasensitive, real-time detection of arginine



Teresa Berninger<sup>a,1</sup>, Christina Bliem<sup>a,1</sup>, Esteban Piccinini<sup>b</sup>, Omar Azzaroni<sup>b,\*</sup>, Wolfgang Knoll<sup>a</sup>

<sup>a</sup> AIT Austrian Institute of Technology GmbH, Biosensor Technologies, Muthgasse 11, 1190 Vienna, Austria

<sup>b</sup> INIFTA Instituto de Investigaciones Físicoquímicas Teóricas y Aplicadas (INIFTA) – Departamento de Química, Facultad de Ciencias Exactas, Universidad Nacional de La Plata – CONICET, Suc. 4, CC 16, La Plata, Argentina

### ARTICLE INFO

#### Keywords:

Enzymatic cascade  
Biosensor  
Arginase  
Urease  
Graphene  
Field-effect transistor

### ABSTRACT

Herein, a biosensor based on a reduced graphene oxide field effect transistor (rGO-FET) functionalized with the cascading enzymes arginase and urease was developed for the detection of L-arginine. Arginase and urease were immobilized on the rGO-FET sensing surface via electrostatic layer-by-layer assembly using polyethylenimine (PEI) as cationic building block. The signal transduction mechanism is based on the ability of the cascading enzymes to selectively perform chemical transformations and prompt local pH changes, that are sensitively detected by the rGO-FET. In the presence of L-arginine, the transistors modified with (PEI/urease(arginase)) multilayers showed a shift in the Dirac point due to the change in the local pH close to the graphene surface, produced by the catalyzed urea hydrolysis. The transistors were able to monitor L-arginine in the 10–1000 μM linear range with a LOD of 10 μM, displaying a fast response and a good long-term stability. The sensor showed stereospecificity and high selectivity in the presence of non-target amino acids. Taking into account the label-free, real-time measurement capabilities and the easily quantifiable, electronic output signal, this biosensor offers advantages over state-of-the-art L-arginine detection methods.

### 1. Introduction

L-arginine ((S)-amino-5-guanidinopentanoic acid) is the most basic amino acid and occurs widely in living organisms. In the human body, it has significant biological functions in the cardiovascular, immune and endocrine system (Guoyao, 2009; Popolo et al., 2014; Tong and Barbul, 2004). The monitoring of L-arginine in physiological fluids is therefore of great interest in clinical diagnostics, research and therapy. Furthermore, it is relevant in industrial settings, such as quality control in food and beverages (Stasyuk et al., 2016; Valle-Vega et al., 1980; Verma et al., 2015) and optimization of microbial biosynthesis in industrial L-arginine production (Ginesy et al., 2015). To date, detection of L-arginine in health-related studies is mostly done by high-performance liquid chromatography (HPLC) (Bode-Böger et al., 1998; Hong et al., 2010; Van Waardenburg et al., 2007) and liquid chromatography-tandem mass spectrometry (LC-MS) (Luneburg et al., 2011; Németh et al., 2016), both of which require specialized equipment and laborious sample preparation and analysis. Optical detection methods may rely on enzymatic reactions (Alonso et al., 1995; Stasyuk et al., 2017, 2016), fluorescent probes (Lu et al., 2017) or functionalized

nanoparticles (Pu et al., 2013; Velugula and Chinta, 2017). Albeit enabling highly sensitive and precise detection, these methods frequently fail to meet many other desirable features such as easy handling, real time response, electronic read-out and cost-efficiency.

As a cutting-edge approach, biosensors based on nanomaterial field-effect transistors (FET) have gained increasing attention in clinical diagnostics because of their following attractive features (Yan et al., 2014): Label-free, real-time response, operation in aqueous solutions at very low voltages (less than 1 V, which is elemental for biological sensing), and inherent amplification property (Zhang et al., 2015). Graphene, a two-dimensional zero band gap semiconducting material, has remarkable electronic, chemical and mechanical properties (Balasubramanian and Kern, 2014; Nehra and Pal Singh, 2015). Its high carrier mobility and ambipolar field effect together with a great interface sensitivity make graphene a unique sensing material. Graphene-based FETs (gFETs) have been applied for detection of pH (Ohno et al., 2009; Reiner-Rozman et al., 2015), DNA (Dong et al., 2010) and proteins (Kim et al., 2013), as well as for the enzymatic detection of small molecules like urea or glucose (Piccinini et al., 2017; Zhang et al., 2015) and other analytes (Fu et al., 2017).

\* Corresponding author.

E-mail address: [azzaroni@inifta.unlp.edu.ar](mailto:azzaroni@inifta.unlp.edu.ar) (O. Azzaroni).

URL: <http://softmatter.quimica.unlp.edu.ar> (O. Azzaroni).

<sup>1</sup> Authors contributed equally and should therefore both be considered first authors.

The approach of enzymatically converting an analyte and detecting it by the resulting small pH changes near the reduced graphene oxide (rGO) surface has successfully been pursued in case of urea (Piccinini et al., 2017). Furthermore, this work reported that electrostatic layer-by-layer (LbL) assemblies offer a versatile bottom-up technique for the immobilization of recognition elements on graphene-modified surfaces, ensuring biological activity and accessibility of the analyte to the active sites of the enzyme.

In the study presented in this paper, we expand this concept to a coupled enzymatic reaction, thereby broadening the spectrum of detectable analytes. For this, the enzymes arginase and urease were immobilized as recognition elements in an LbL assembly on reduced graphene oxide field effect transistors (rGO-FET), thus enabling a highly sensitive, precise and selective detection of L-arginine. In the first reaction step of this cascading set-up, arginase hydrolyzes L-arginine to yield ornithine and urea, none of which provoke a sensor response. The intermediate urea serves as a substrate for the second reaction step, in which it is converted by urease into NH<sub>3</sub> and CO<sub>2</sub>, thus leading to an increase in pH on the rGO-FET surface. Optimizing the LbL architecture, biosensors with a very low limit of detection (LOD) of < 10 μM, a wide linear range of 10–1000 μM and rapid response time of 180 s were obtained. Featuring these characteristics, our biosensor compares favorably with those described in the literature. Furthermore, our study is the first one describing the construction of an enzymatic cascade in an LbL assembly on an rGO-FET, thus paving the way for other sequential enzymes to potentially be applied as cascading recognition elements in biosensors.

## 2. Material and methods

### 2.1. Chemicals

For the experiments performed in this study, the following reagents were used: L-arginase (Ar) from bovine liver (100 units/mg, Calzyme Laboratories Inc., San Luis Obispo, CA, USA), urease (Ur) from Jackbean (*Canavalia ensiformis*) (100 units/mg, Calzyme) and dimethylformamide (DMF) (Research AG, Argentina). L-arginine monohydrochloride, D-arginine monohydrochloride, L-canavanine, L-valine, L-alanine, creatinine, L-phenylalanine, L-proline, hydrazine monohydrate (99%), (3-aminopropyl)-triethoxysilane (APTES) (97%), sodium 1-pyrenesulfonate (SPS), polyethyleneimine (PEI) (Mw 10,000) and urea (all from Sigma-Aldrich, USA). Interdigitated microelectrodes (ED-IDE1-Au) as well as the electrochemical flow cell were obtained from Micrux Technologies (Oviedo, Spain). Ultrapure Milli-Q water was used to prepare all the solutions.

### 2.2. Preparation of reduced graphene oxide field effect transistors (rGO-FETs) and layer-by-layer assembly

As a first step, rGO-FETs as transducing platforms were prepared as described in Piccinini et al. (2017). To functionalize the rGO-FETs for sensing applications, the enzymes were integrated on the rGO platform via electrostatic layer-by-layer (LbL) assembly in the presence of polyethyleneimine (PEI). The use of the polyelectrolyte has three distinctive advantages: 1) weak polyelectrolytes amplify the pH sensitivity by protonation and deprotonation of the monomer units, thus resulting in electrostatic gating (Piccinini et al., 2017), 2) they increase the interfacial sensitivity of gFETs (Piccinini and Alberti et al., 2018) and 3) they act as supramolecular building blocks (Ariga et al., 2014, 2007; Decher and Hong, 1991). The enzyme solutions were prepared in 10 mM HEPES + 10 mM KCl aqueous buffer and pH was adjusted above their isoelectric points. The solutions contained either 1 mg/ml of urease or arginase respectively or a mixture of both enzymes in a ratio of 1:1 or 1:2, maintaining the total enzyme concentration of 1 mg/ml constant. The rGO-functionalized microelectrodes were immersed in a solution of 5 mM SPS in DMF overnight, conferring negative surface

charge. After rinsing with DMF and water, the first polycation layer was assembled submerging the rGO-FETs for 10 min in a 2 mg/ml aqueous PEI solution (adjusted to pH 8). Subsequently, the rGO-FETs were rinsed with water and transferred into the enzyme solution for 30 min. Unbound enzymes were carefully washed off by rinsing with water. Different LbL-architectures were obtained by repeating the alternating steps of polycation and enzyme adsorption and varying the ratio of arginase and urease as desired. The functionalized rGO-FETs were used for electrochemical measurements immediately.

### 2.3. Surface plasmon resonance (SPR) spectroscopy

Basic piranha solution (H<sub>2</sub>O<sub>2</sub> 30% and NH<sub>4</sub>OH 35% 1:1) was used to clean gold SPR substrates (SPR102 AU, BioNavis) by heating at 60 °C for 10 min. The SPR substrates were first modified with cysteamine and then with rGO as previously reported (Piccinini and Alberti et al., 2018). The rGO-modified substrates were washed with water and dried with N<sub>2</sub>. The assembly process involving the sequential adsorption of PEI, urease and arginase adsorption was monitored using the multi-parametric surface plasmon resonance (MP-SPR) instrument SPR Navi 210 A (BioNavis Ltd, Tampere, Finland). The measurements were carried out using a 785 nm laser and a flow rate of 10 μl/min. To estimate the surface coverage of the biocomponents, the SPR angle of minimum reflectivity, θ<sub>min</sub>, was measured in situ during the assembly. The shift of the minimum reflectivity angle (Δθ) resulting from the adsorption of each enzyme was converted into mass surface coverage (Γ, ng/cm<sup>2</sup>) using the following equation (Stenberg et al., 1991):

$$\Gamma = \frac{\Delta\theta kd}{d\eta/dC} \quad (1)$$

The parameter k\*d, which depends on the SPR substrate and the wavelength of the laser, was provided by BioNavis with a value of 1.9 × 10<sup>-7</sup> cm/deg. The refractive-index variation (η) with concentration (C), i.e.: (dη/dC), was considered equal for urease and arginase with a value of 1.82 × 10<sup>-10</sup> cm<sup>3</sup>/ng (Zhao et al., 2011).

### 2.4. Electrochemical L-arginine detection

Real time measurements were performed using the functionalized rGO-FETs. They were inserted into the electrochemical flow cell to perform the measurements in a liquid gated configuration with a silver wire as gate electrode. All analytes (L-arginine and non-target amino acids) were prepared in a 10 mM KCl buffer adjusted to pH 6. The analyte solutions were continuously injected by a peristaltic pump at a flow rate of 100 μl/min (Reglo ICC, Ismatec, Cole-Parmer GmbH, Wertheim, Germany). The current between source and drain electrodes (I<sub>D</sub>) was monitored by applying a source-drain bias (V<sub>ds</sub>) of 0.1 V and a fixed gate voltage (V<sub>g</sub>) of -0.2 V. The term ΔI<sub>D</sub> refers to the variation in I<sub>D</sub> upon adding the analyte to the working solution.

## 3. Results and discussion

### 3.1. Characterization of the rGO-FETs

Liquid gated FETs using rGO as a channel material were used as sensing platforms (Fig. 1a). The bridging of source and drain electrode by the randomly organized rGO flakes is facilitated by the special architecture with a small channel length (10 μm), resulting in an extremely high transconductance of up to 800 μS (Piccinini et al., 2017) as well as a stable response and high device to device reproducibility.

We recently reported the outstanding sensitivity of electrolyte solution-gated rGO-FETs towards pH changes near the rGO surface exhibiting a broad linear range with a slope of 20.3 ± 0.6 μA/pH (Piccinini et al., 2017). This phenomenon arises from two effects: 1) changes in the surface charge density by the protonation or deprotonation of remaining functional groups at the rGO surface and the charge

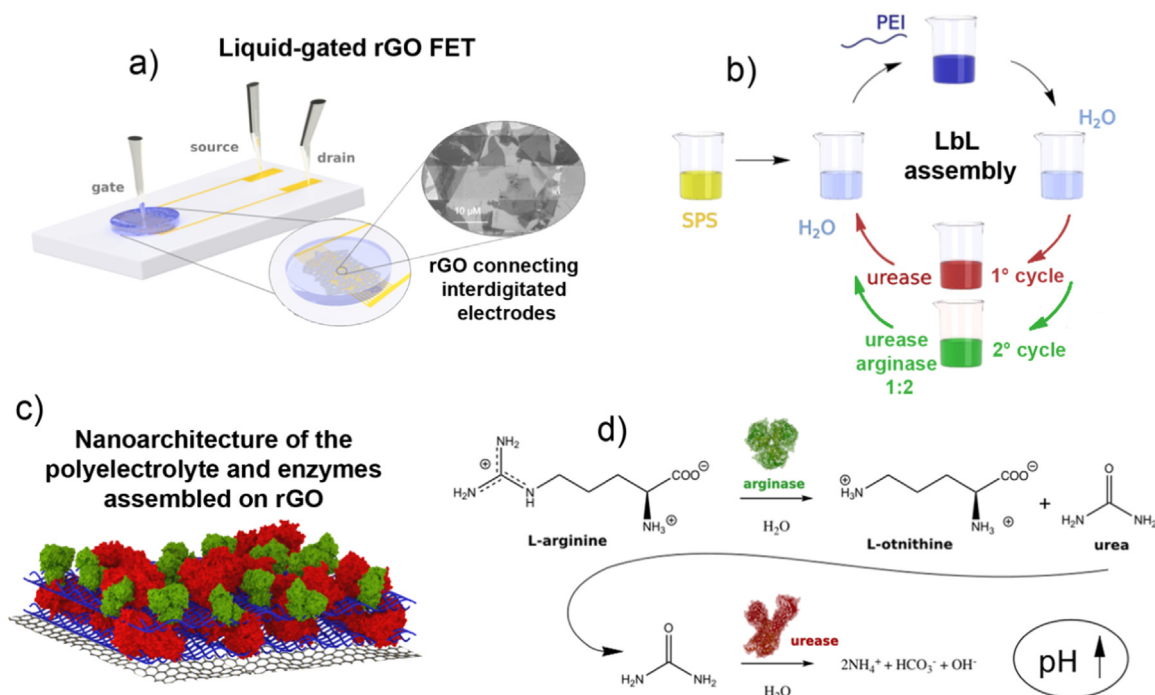


**Fig. 1.** a) Illustration of the liquid gated gFET with source, drain and gate electrode, an enlarged view of the interdigitated channel and a SEM image of the rGO modified channel; scale bar = 10  $\mu\text{M}$ . b) Schematic of the LbL assembly process using PEI as the cationic building block, and urease (for the 1<sup>o</sup> cycle) and urease:arginase 1:2 (for the 2<sup>o</sup> cycle) as the anionic building blocks. c) Representation of the LbL assembly of PEI (blue), urease (red) and arginase (green). d) Reaction equation of the conversion of L-arginine into L-ornithine and the intermediate substrate urea by the enzyme arginase (EC 3.5.3.1., green) and the following urease (EC 3.5.1.5., red)-catalyzed hydrolysis of urea. (For the color version of all the figures, the reader is referred to the online version of this article.).

doping effect of adsorbed  $\text{H}^+$  or  $\text{OH}^-$  ions and 2) electrostatic gating effects due to changes in the Debye layer (Heller et al., 2010; Sohn et al., 2013; Wang and Burke, 2014). By integrating the weak polycation polyethylenimine (PEI) with a pKa of 8–9, the pH sensitivity of the device has been enhanced by 28%. This was due to the deprotonation of PEI when increasing the pH, resulting in p-doping of the transducer by electrostatic gating effects (Piccinini et al., 2017). This pH sensitivity, together with the ease of fabrication and low cost, makes the developed rGO-FETs highly suitable to be used as biosensing platforms.

### 3.2. Immobilization of enzymes using the layer-by-layer (LbL) assembly technique

Enzymes were immobilized on the sensing platform using the LbL technique, which relies on the electrostatic interaction of the polycation PEI and the enzymes (Fig. 1b,c). This method overcomes the constraints of standard covalent attachment, which might disrupt the folding and functionality of the enzymes if essential groups are involved in the immobilization (Scouten et al., 1995; Sheldon and van Pelt, 2013). In addition, direct covalent attachment to the graphene surface can induce the damage to the  $\text{sp}^2$  structure and thus impair signal transduction (Niyogi et al., 2010). The use of polyelectrolytes allow for precise tuning of the enzyme spacing and loading within the assembly as well as to optimizing the enzyme ratio (Ariga et al., 2013), which is of great importance in multistep cascade reactions.

Before assembling the initial layer of PEI, a negative charge was conferred to the rGO surface by using sodium 1-pyrenesulfonate (SPS) as a priming layer. In the assembly process, the pH of the polyelectrolyte and enzyme solution is critical. Enzymes are negatively charged at a pH above their characteristic isoelectric point (pI), which is required for their electrostatic adsorption to the positively charged PEI. To identify a suitable pH, the adsorption process of PEI and enzymes onto the rGO-modified substrates was followed by SPR at enzyme buffer pH of 7.4 or 8.5. Fig. 2 shows the reflectivity curves after the adsorption

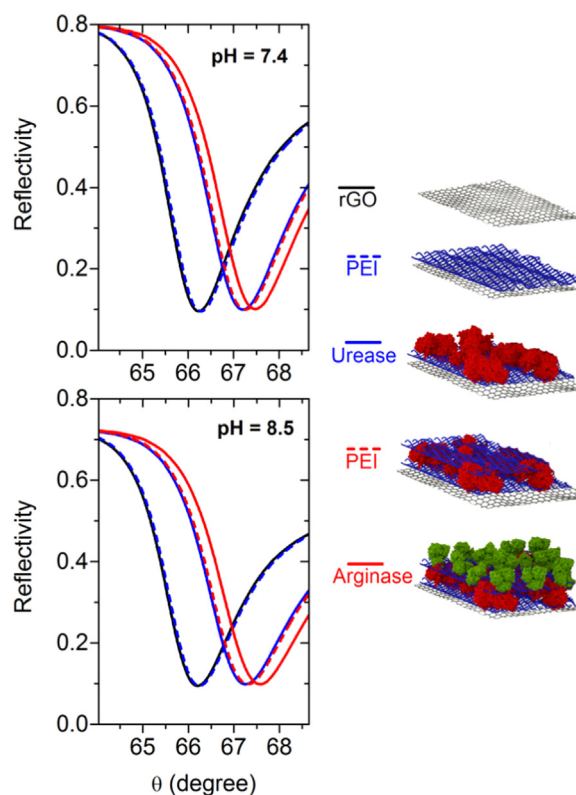


**Fig. 2.** SPR reflectivity curves of the LbL assembly of PEI (dashed blue), urease (blue), PEI (dashed red) and arginase (red) onto rGO (black) at pH 7.4 (top) and 8.5 (bottom). (For interpretation of the references to color in this figure legend, the reader is referred to the web version of this article.).

and rinsing of each component. SPR measurements confirmed the successful assembly of the enzymes and a high stability of the whole supramolecular interfacial architecture. The surface coverage ( $\Gamma$ ) of the enzymes was calculated applying Eq. (1) described in the methods section. By increasing the pH of the arginase buffer to 8.5, the loaded arginase increased by 20% compared to adsorption at pH 7.4. Surface coverage values of 1054 and 292 ng/cm<sup>2</sup> were obtained for urease and arginase, respectively, when the proteins were assembled at pH 8.5. Since pH 8.5 increased arginase adsorption and did not impede urease functionality (Figs. S4 and S5 in the Supporting information file), the enzyme buffer was adjusted to this value in all further LbL assemblies.

### 3.3. Sensing performance depending on LbL architecture

Due to their outstanding selectivity, enzymes were used as biorecognition elements on the rGO FETs. The change in the local pH at the transducer surface upon analyte conversion can be correlated to the substrate concentration (Lee et al., 2009; Piccinini et al., 2017; Sohn et al., 2013; Soldatkin et al., 2002). By sequentially coupling enzymes, the scope of detectable analytes can be extended. This is particularly true for the cascading enzymatic arrangement of arginase and urease to detect L-arginine (Fig. 1d). The first reaction, catalyzed by arginase, leads to the formation of L-ornithine and urea. Neither of these intermediates are pH active, however, urea is the substrate for the following urease-catalyzed reaction into NH<sub>4</sub><sup>+</sup>, HCO<sub>3</sub><sup>-</sup> and OH<sup>-</sup>. Thus, the coupling of both enzymes leads to an pH increase in the presence of L-arginine. At negative V<sub>g</sub>, the local accumulation of OH<sup>-</sup> induces an

increase in the hole carrier concentration, which is recorded as an increase in I<sub>D</sub> (Fig. 3a,b).

The assembly architecture containing the enzymes is highly relevant for the sensing performance, especially when dealing with cascading enzymatic reactions (Disawal et al., 2003; Pescador et al., 2008). The immobilization process should prevent the leakage of the enzyme (Saiapina et al., 2012) and ensure the substrate accessibility. To identify the optimum LbL architecture, different multilayer arrangements were examined in order to elucidate the best sensing performance (Figs S4 and S5 in the Supporting information file). We observed that the configuration PEI-Ur-PEI-UrAr-PEI (Ur:Ar 1:2) exhibits the best performance in comparison with PEI-Ur-PEI-UrAr-PEI (Ur:Ar 1:1) and PEI-UrAr-PEI.

The close proximity of both enzymes participating in a cascade reaction is crucial for optimal catalytic conversion of the analyte (Fu et al., 2012; Kang et al., 2014; Pescador et al., 2008). Fu et al. (2012) attributed this phenomenon to the facilitated transport of the intermediate along the protein surfaces as opposed to diffusion through the bulk solution, whereas other authors argue that the enhanced activity is due to a positive effect of close entrapment in the scaffold on kinetic parameters, for example by changes in the pH of the microenvironment (Zhang and Hess, 2017).

Therefore, the enzymes urease and arginase were co-immobilized in the outermost layer of the assembly. Furthermore, urease was incorporated in the assembly in excess by including a bottom layer entirely constituted of urease (rGO-pyrSO<sub>3</sub>/PEI/Urease/PEI/Urease + Arginase/PEI), thus preventing unspecific interaction of the

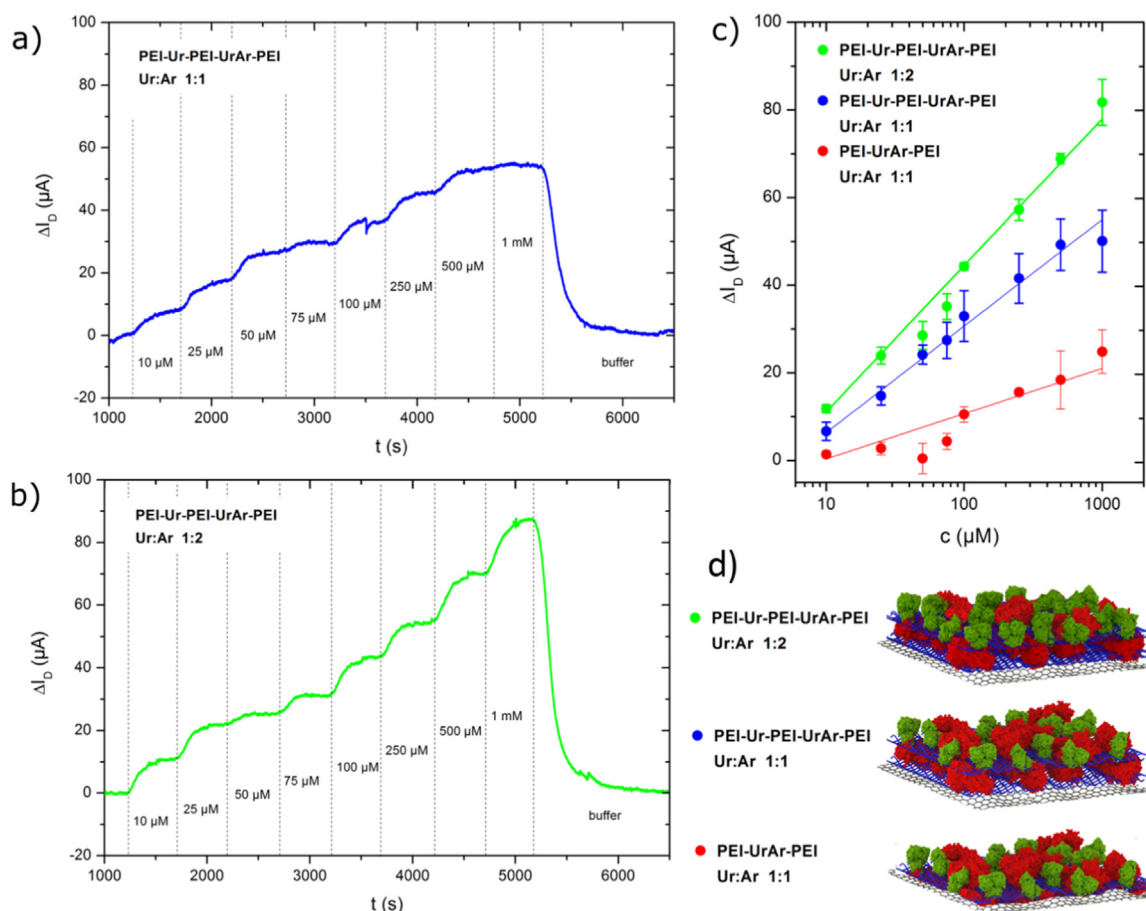


**Fig. 3.** a) Real-time channel current response ( $\Delta I_D$ ) for the PEI-Ur-PEI-UrAr-PEI assembly with a ratio of Ur:Ar of 1:1 b) and Ur:Ar 1:2 in the outermost enzyme layer. The dashed lines represent the change in concentration. c)  $\Delta I_D$  response of the assemblies PEI-UrAr-PEI Ur:Ar 1:1 ( $R = 0.90$ ) (red), PEI-Ur-PEI-UrAr-PEI Ur:Ar 1:1 ( $R = 0.99$ ) (blue) and PEI-Ur-PEI-UrAr-PEI Ur:Ar 1:2 ( $R = 0.99$ ) (green). Error bars represent the standard deviation of three measurements. Experimental conditions: 10 mM KCl at pH 6, V<sub>g</sub>: -0.2 V, V<sub>sd</sub>: 0.1 V, flow rate: 100  $\mu l/min$ . (For interpretation of the references to color in this figure legend, the reader is referred to the web version of this article.)

transducing element with charged intermediate products due to incomplete enzymatic conversion, which may lower the signal of the transistor. This configuration allowed the real time detection of arginine, with a detection limit of 10  $\mu\text{M}$ , a linear range from 10  $\mu\text{M}$  to 1000  $\mu\text{M}$  and a slope of 24  $\mu\text{A}$  per decade [L-arginine] when both enzymes were integrated in a 1:1 ratio (Fig. 3a,c).

In addition to proximity, the ratio between both enzymes has been suggested as an effective approach to optimize the bi-enzymatic cascade reaction (Zhang and Hess, 2017). In order to ensure sufficient analyte conversion and thus intermediate substrate concentration, the urease:arginase ratio was increased to 1:2 in the outermost enzyme layer of the assembly. However, owing to the additional urease layer, the concentration of urease was kept higher within the entire assembly. In the two-step hydrolysis of L-arginine, urease is known to be the rate-limiting enzyme due to its lower  $K_m$  and thus lower maximum reaction rate  $V_{\text{max}}$  compared to arginase for the same amount of enzymatic units (Liu et al., 1996). Therefore, the application of urease in excess has been suggested to ensure a prompt conversion of all intermediate species and render the observed rate of ammonia formation directly proportional to the concentration of arginine (Liu et al., 1996).

For the optimized assembly we could observe an enhanced sensitivity towards the analyte with a slope of 33.5  $\mu\text{A}$  per decade and a linear range between 10 and 1000  $\mu\text{M}$  (3b,c). The sensitivity decayed above 1000  $\mu\text{M}$  arginine due to the saturation of the enzymatic activity. A dilution of the sample should be done to measure above this concentration. The presented sensor outperforms most of the urease/arginase based potentiometric sensors reported in the literature with respect to its LOD, linear working range and response time (see Table 1). In this sense, we should note that while the conductometric sensor presented by Saiapina et al. (2012) displayed a lower LOD and a slightly faster response time, our rGO-FET based sensor has the advantage of enabling measurements in continuous flow conditions and, thus, achieving a real-time detection of the analyte. Furthermore, the biosensor response was completely reversible, which was shown by injecting buffer solution subsequent to analyte titration, resulting in the decrease of  $I_D$  to reach the initial baseline value. This indicated the absence of undesirable, unspecific adsorption of substrate or products near the surface of the rGO-FET, which would have altered its charge carrier mobility and thereby also  $I_D$ . The use of the LbL technique for enzyme immobilization offers the opportunity of closely controlling the nanoarchitecture of the assembly as opposed to other methods involving covalent chemistries such as cross-linking the bi-enzyme solution. This is not only relevant in the case of our arginine biosensor, but may also serve as a model approach for the study of other multienzyme systems and their microenvironments. By optimizing the composition of the LbL assembly the working stability of the sensor could be improved, resulting in a low standard deviation within measurements. A comparison with other sensing strategies reveals that the response time of our platform is faster than other arginine sensors. The response was very rapid, reaching 95% of the maximum value within the initial 180 s. This is opposed to the slow substrate conversion of free enzymes in

buffer, indicating a successful enhancement of catalytic activity by enzyme immobilization using polyelectrolytes in a multilayer architecture.

The linear range of our device covers typical concentrations in real samples. L-arginine concentration in human plasma normally lies between 40 and 110  $\mu\text{M}$  (Lunenburg et al., 2011). However, it can reach up to 1.2 mM after oral ingestion and even higher values of up to 7.7 mM after intravenous infusion (Bode-Böger et al., 1998). Also, L-arginine levels in food samples or industrial production may exceed the upper limit of the linear range of our biosensor. However, the linear range can be shifted by adjusting the operating conditions. For example, increasing the buffer capacity in the working buffer was reported to render the biosensor less sensitive, but resulted in a linear response up to higher concentrations (Saiapina et al., 2012). Therefore, it is envisaged the application of the developed biosensor in a variety of settings involving different matrices.

To investigate the selectivity of the biosensor towards L-arginine, a range of non-target amino acids was studied. To this end, the response of rGO-FETs modified with the optimized LbL architecture (rGO-pyrSO<sub>3</sub>/PEI/Urease/PEI/Urease + Arginase/PEI) was evaluated in the presence of L-valine, L-alanine, creatinine and L-phenylalanine. The sensor showed no or very little response (max. 3  $\mu\text{A}$ ) to non-target amino acids even at high concentrations (100  $\mu\text{M}$  and 1 mM) (Fig. 4). Furthermore, stereospecificity was confirmed by exposing the sensor to D-arginine solutions. This control experiment in the presence of 100  $\mu\text{M}$  D-arginine resulted in approximately a 5  $\mu\text{A}$  decrease in  $\Delta I_D$  (Fig. 4b). Since the resulting signal (decrease in  $\Delta I_D$ ) of these non-target amino acids was in contrast to the one by L-arginine (increase in  $\Delta I_D$ ), none of them is expected to yield a false positive response.

Recent works (Fu et al., 2017; Piccinini et al., 2018) explained that the electrostatic screening by mobile ions (Debye length) is an important limitation in graphene-based FETs if real samples such as serum need to be measured. This drawback applies when the sensing mechanism is the induction of a local electric field produced by the charged target molecule (e.g., DNA, antigen, proteins, etc.) recognized on the graphene surface. Since the sensing mechanism used in this work is based on the acid/base equilibrium of the products of an enzymatic reaction, the above mentioned issue is not a limitation for our sensors. Nevertheless, the sensor surface should be engineered to avoid the fouling of proteins on the film using different building blocks such as PEG or zwitterionic polymers.

#### 4. Conclusion

We described a novel, highly sensitive biosensing platform to detect L-arginine. The biosensor has been designed and built employing the enzymatic cascade of arginase and urease as recognition elements. These enzymes were immobilized on an rGO-FET by employing the LbL technique. By evaluating the performance of different LbL architectures, it has been concluded that the enzyme ratio and the proximity between arginase and urease represent key factors. Our experiments

**Table 1**

Overview of electrochemical L-arginine biosensors based on enzyme coupling described in the literature.

Biological recognition element	Method	LOD mM	Linear range mM	Response time	Reference
Urease/Arginase	Amperometric	0.038	0.07–0.6	10 s	(Stasyuk et al., 2012)
Urease/Arginase	Conductometric	0.0005	0.01–4	120 s	(Saiapina et al., 2012)
Urease/Arginase	Potentiometric		0.03–3	300 s	(Nikolelis and Hadjiioannou, 1983)
Urease/Arginase	Potentiometric	< 0.01	0.1–30	90–360 s (95%)	(Koncki et al., 1996)
Urease/Arginase	Potentiometric		0.025–0.310	600 s	(Karacaoğlu et al., 2003)
Urease/Arginase	Potentiometric	0.1	0.12 – 40	180–300 s (95%)	(Stasyuk et al., 2011)
Urease/Arginase	Potentiometric		0.1–10	300 s	(Valle-Vega et al., 1980)
Urease/Arginase	Potentiometric		mM range		(Disawal et al., 2003)
Urease/Arginase	Potentiometric		0.01–1		(Komaba et al., 1998)
Urease/Arginase	Potentiometric		0.1–1		(Ivnitskii and Rishpon, 1993)
Urease/Arginase	FET	0.01	0.01–1	180 s	This work

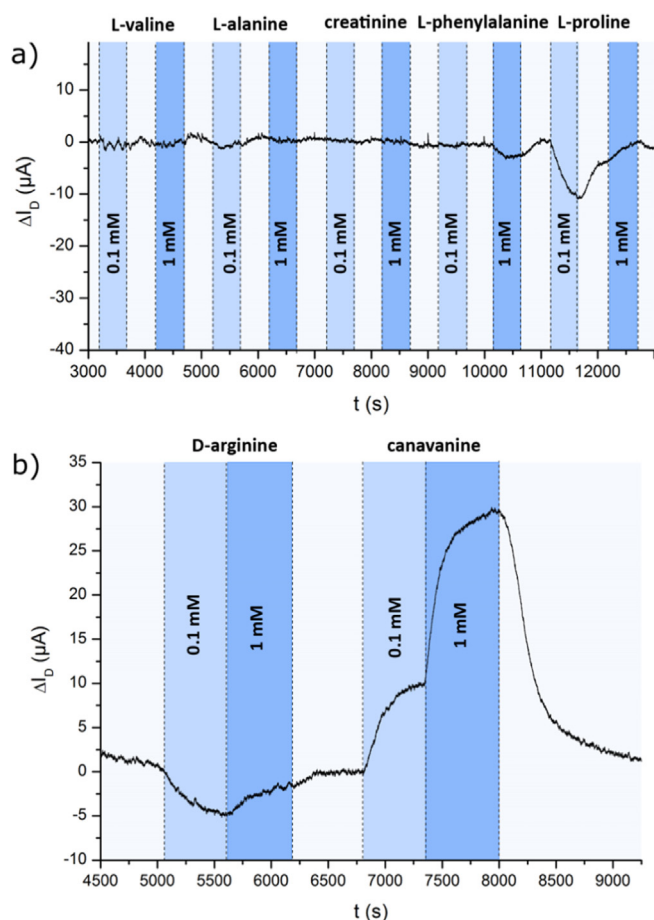


**Fig. 4.** a) Real-time channel current response ( $\Delta I_d$ ) for the LbL assembly PEI-Ur-PEI-Ur:Ar 1:2 titrating different interfering species: L-valine, L-alanine, Creatinine, L-phenylalanine, L-proline as well as b) D-arginine and canavanine at concentrations of 100  $\mu$ M (light blue) and 1 mM (blue). The dashed lines represent the change in concentration. Experimental conditions: 10 mM KCl at pH 6,  $V_g$ :  $-200$  mV,  $V_{sd}$ : 100 mV, flow rate: 100  $\mu$ l/min. (For interpretation of the references to color in this figure legend, the reader is referred to the web version of this article.)

revealed that the best sensing performance was achieved by those assemblies containing only urease in the inner bioactive layer and both enzymes (Ur:Ar 1:2) in the outer bioactive layer (rGO-pyrSO<sub>3</sub>/PEI/Urease/PEI/Urease + Arginase 1:2/PEI). As a result, a sensing platform exhibiting fast response (180 s), a linear range between 10  $\mu$ M and 1 mM, a LOD of 10  $\mu$ M, and a sensitivity of 33  $\mu$ A/ $\mu$ M was obtained. We envision that further exploration of this strategy relying on the use of enzymatic cascades to other enzymatic systems will open up new opportunities to highly sensitive graphene-based sensors.

#### Acknowledgements

This work was supported by the European Union's Horizon 2020 under the Marie Curie Grant agreement no. 645686, CONICET (PIP 0370), ANPCyT (PICT-2013-0905, PICT-2016-1680), the Austrian Institute of Technology GmbH (AIT-CONICET Partner Group, Exp. 4947/11, Res. No. 3911, 28-12-2011), Universidad Nacional de La Plata (UNLP) (PPID-X016), the Austrian Federal Ministry for Transportation, Innovation and Technology (GZ BMVIT-612.166/0001-III/11/2010), by the FFG within the comet program, and from the governments of Lower and Upper Austria. E.P. acknowledges CONICET for a scholarship. C.B. acknowledges the financial support given by the NÖ Forschungs- und Bildungsges.m.b.H. O.A. is a staff researcher of CONICET. We thank Josef Breu for supplying graphene oxide flakes.

#### Conflict of interest

The authors have no conflict of interest to declare.

#### Appendix A. Supporting information

Supplementary data associated with this article can be found in the online version at <http://dx.doi.org/10.1016/j.bios.2018.05.027>.

#### References

- Alonso, A., Almendral, M.J., Báez, M.D., Porras, M.J., Alonso, C., 1995. *Anal. Chim. Acta* 308, 164–169.
- Ariga, K., Hill, J.P., Ji, Q., 2007. *Phys. Chem. Chem. Phys.* 9, 2319–2340.
- Ariga, K., Ji, Q., Mori, T., Naito, M., Yamauchi, Y., Abe, H., Hill, J.P., 2013. *Chem. Soc. Rev.* 42, 6322.
- Ariga, K., Yamauchi, Y., Rydzek, G., Ji, Q., Yonamine, Y., Wu, K.C.-W., Hill, J.P., 2014. *Chem. Lett.* 43, 36–68.
- Balasubramanian, K., Kern, K., 2014. *Adv. Mater.* 26, 1154–1175.
- Bode-Böger, S.M., Böger, R.H., Galland, A., Tsikas, D., Frölich, J.C., 1998. *Br. J. Clin. Pharmacol.* 46, 489–497.
- Decher, G., Hong, J.D., 1991. *Ber. Bunsenges. Phys. Chem.* 95, 1430–1434.
- Disawal, S., Qiu, J., Elmore, B.B., Lvov, Y.M., 2003. *Colloids Surf. B* 32, 145–156.
- Dong, X., Shi, Y., Huang, W., Chen, P., Li, L.J., 2010. *Adv. Mater.* 22, 1649–1653.
- Fu, J., Liu, M., Liu, Y., Woodbury, N.W., Yan, H., 2012. *J. Am. Chem. Soc.* 134, 5516–5519.
- Fu, W., Jiang, L., van Geest, E.P., Lima, L.M.C., Schneider, G.F., 2017. *Adv. Mater.* 29, 1603610.
- Ginesy, M., Belotserkovsky, J., Enman, J., Isaksson, L., Rova, U., 2015. *Microb. Cell Fact.* 14, 29.
- Guoyao, W., 2009. *Aminoacids* 37, 153–168.
- Heller, I., Chatoor, S., Männik, J., Zevenbergen, M.A.G., Dekker, C., Lemay, S.G., 2010. *J. Am. Chem. Soc.* 132, 17149–17156.
- Hong, S.K.S., Maltz, B.E., Coburn, L.A., Slaughter, J.C., Chaturvedi, R., Schwartz, D.A., Wilson, K.T., 2010. *Inflamm. Bowel Dis.* 16, 105–111.
- Ivinskii, D.M., Rishpon, J., 1993. *Anal. Chim. Acta* 282, 517–525.
- Kang, W., Liu, J., Wang, J., Nie, Y., Guo, Z., Xia, J., 2014. *Bioconjug. Chem.* 25, 1387–1394.
- Karacaoğlu, S., Timur, S., Telefoncu, A., 2003. *Artif. Cells Blood Substit. Immobil. Biotechnol.* 31, 357–363.
- Kim, D.J., Sohn, I.Y., Jung, J.H., Yoon, O.J., Lee, N.E., Park, J.S., 2013. *Biosens. Bioelectron.* 41, 621–626.
- Komaba, S., Fujino, Y., Matsuda, T., Osaka, T., Satoh, I., 1998. *Sens. Actuatur., B Chem.* 52, 78–83.
- Koncki, R., Walcerz, I., Ruckruh, F., Glab, S., 1996. *Anal. Chim. Acta* 333, 215–222.
- Lee, C.S., Kyu Kim, S., Kim, M., 2009. *Sensors* 9, 7111–7131.
- Liu, D., Nie, L., Yao, S., 1996. *Talanta* 43, 667–674.
- Lu, W., Gao, Y., Jiao, Y., Shuang, S., Li, C., Dong, C., 2017. *Nanoscale* 9, 11545–11552.
- Lunenburg, N., Xanthakis, V., Schwedhelm, E., Sullivan, L.M., Maas, R., Anderssohn, M., Riederer, U., Glazer, N.L., Vasan, R.S., Boger, R.H., 2011. *J. Nutr.* 141, 2186–2190.
- Nehra, A., Pal Singh, K., 2015. *Biosens. Bioelectron.* 74, 731–743.
- Németh, B., Kiss, I., Péter, I., Ajtay, Z., Németh, Á., Márk, L., Csorba, A., Keszegi, T., Műhl, D., Kustán, P., 2016. *In Vivo* 30, 663–670.
- Nikolelis, D.P., Hadjiioannou, T.P., 1983. *Anal. Chim. Acta* 147, 33–39.
- Niyogi, S., Bekyarova, E., Itkis, M.E., Zhang, H., Shepperd, K., Hicks, J., Sprinkle, M., Berger, C., Lau, C.N., Deheer, W.A., Conrad, E.H., Haddon, R.C., 2010. *Nano Lett.* 10, 4061–4066.
- Ohno, Y., Maehashi, K., Yamashiro, Y., Matsumoto, K., 2009. *Nano Lett.* 9, 3318–3322.
- Pescador, P., Katakis, I., Toca-Herrera, J.L., Donath, E., 2008. *Langmuir* 24, 14108–14114.
- Piccinini, E., Alberti, S., Longo, G.S., Berninger, T., Breu, J., Dostalek, J., Azzaroni, O., Knoll, W., 2018. *J. Phys. Chem. C*. <http://dx.doi.org/10.1021/acs.jpcc.7b11128>.
- Piccinini, E., Bliem, C., Reiner-Rozman, C., Battaglini, F., Azzaroni, O., Knoll, W., 2017. *Biosens. Bioelectron.* 92, 661–667.
- Popolo, A., Adesso, S., Pinto, A., Autore, G., Marzocco, S., 2014. *Amino Acids* 46, 2271–2286.
- Pu, W., Zhao, H., Huang, C., Wu, L., Xu, D., 2013. *Anal. Chim. Acta* 764, 78–83.
- Reiner-Rozman, C., Larisika, M., Nowak, C., Knoll, W., 2015. *Biosens. Bioelectron.* 70, 21–27.
- Saiaipina, O.Y., Dzyadevych, S.V., Jaffrezic-Renault, N., Soldatkin, O.P., 2012. *Talanta* 92, 58–64.
- Scouten, W.H., Luong, J.H.T., Stephen Brown, R., 1995. *Trends Biotechnol.* 13, 178–185.
- Sheldon, R.A., van Pelt, S., 2013. *Chem. Soc. Rev.* 42, 6223–6235.
- Sohn, I.Y., Kim, D.J., Jung, J.H., Yoon, O.J., Nguyen Thanh, T., Tran Quang, T., Lee, N.E., 2013. *Biosens. Bioelectron.* 45, 70–76.
- Soldatkin, A.P., Montoriol, J., Sant, W., Martelet, C., Jaffrezic-Renault, N., 2002. *Talanta* 58, 351–357.
- Stasyuk, N., Gayda, G., Yepremyan, H., Stepien, A., Gonchar, M., 2017. *Acta A* 170, 184–190.
- Stasyuk, N., Smutok, O., Gayda, G., Gonchar, M., 2011. *J. Mater. Sci. Eng.* 1, 819–827.
- Stasyuk, N., Smutok, O., Gayda, G., Vus, B., Koval'chuk, Y., Gonchar, M., 2012. *Biosens. Bioelectron.* 37, 46–52.

- Stasyuk, N.Y., Gayda, G.Z., Fayura, L.R., Boretskyy, Y.R., Gonchar, M.V., Sibirny, A.A., 2016. *Food Chem.* 201, 320–326.
- Stenberg, E., Persson, B., Roos, H., Urbaniczky, C., 1991. *J. Colloid Interface Sci.* 143, 513–526.
- Tong, B., Barbul, A., 2004. *Mini Rev. Med. Chem.* 4, 823–832.
- Valle-Vega, P., Young, C.T., Swaisgood, H.E., 1980. *J. Food Sci.* 45, 1026–1030.
- Van Waardenburg, D.A., De Betue, C.T., Luiking, Y.C., Engel, M., Deutz, N.E., 2007. *Am. J. Clin. Nutr.* 86, 1438–1444.
- Velugula, K., Chinta, J.P., 2017. *Biosens. Bioelectron.* 87, 271–277.
- Verma, N., Singh, A.K., Kaur, P., 2015. *J. Anal. Chem.* 70, 1111–1115.
- Wang, Y.Y., Burke, P.J., 2014. *Nano Res.* 7, 1650–1658.
- Yan, F., Zhang, M., Li, J., 2014. *Adv. Healthc. Mater.* 3, 313–331.
- Zhang, M., Liao, C., Mak, C.H., You, P., Mak, C.L., Yan, F., 2015. *Sci. Rep.* 5, 1–6.
- Zhang, Y., Hess, H., 2017. *ACS Catal.* 7, 6018–6027.
- Zhao, H., Brown, P.H., Schuck, P., 2011. *Biophys. J.* 100, 2309–2317.